J Biomol NMR (2010) 48:103–111
DOI 10.1007/s10858-010-9442-8

ARTICLE

High resolution ^{13}C-detected solid-state NMR spectroscopy of a deuterated protein

Ming Tang · Gemma Comellas · Leonard J. Mueller · Chad M. Rienstra

Received: 14 July 2010 / Accepted: 30 July 2010 / Published online: 29 August 2010

Abstract High resolution ^{13}C-detected solid-state NMR spectra of the deuterated beta-1 immunoglobulin binding domain of the protein G (GB1) have been collected to show that all ^{15}N, ^{13}C′, ^{13}Cα and ^{13}Cβ sites are resolved in ^{13}C–^{13}C and ^{15}N–^{13}C spectra, with significant improvement in T_2 relaxation times and resolution at high magnetic field (750 MHz). The comparison of echo T_2 values between deuterated and protonated GB1 at various spinning rates and under different decoupling schemes indicates that ^{13}Cα T_2' times increase by almost a factor of two upon deuteration at all spinning rates and under moderate decoupling strength, and thus the deuteration enables application of scalar-based correlation experiments that are challenging from the standpoint of transverse relaxation, with moderate proton decoupling. Additionally, deuteration in large proteins is a useful strategy to selectively detect polar residues that are often important for protein function and protein–protein interactions.

Keywords Deuterated protein · Solid-state NMR · ^{13}C-detected spectra · Deuterium effect · T_2' relaxation rates

Abbreviations used

DARR	Dipolar assisted rotational resonance
GB1	The beta-1 immunoglobulin binding domain of protein G
MAS	Magic-angle spinning
SSNMR	Solid-state nuclear magnetic resonance
CTUC COSY	Constant time uniform-sign cross-peak correlation spectroscopy
IPAP	In-phase anti-phase

Introduction

Deuteration is a common strategy employed in protein solution NMR to improve the spectral resolution and sensitivity by increasing the transverse relaxation times (T_2) and suppressing the ^{1}H–^{1}H scalar couplings (Gardner and Kay 1998). The combination of triple resonance experiments with ^{2}H, ^{13}C, ^{15}N labeled samples is essential for the solution structure determination of large proteins, but the substitution of deuterons for protons depletes the number of protons available for distance restraints. As a result, several deuterium-labeling schemes that produce molecules with different patterns of incorporation have been employed (Gardner and Kay 1998).

The authors Ming Tang and Gemma Comellas contributed equally to this work.

M. Tang · C. M. Rienstra (✉)
Department of Chemistry, University of Illinois at Urbana-Champaign, 600 South Mathews Avenue, Urbana, IL 61801, USA
e-mail: rienstra@scs.uiuc.edu

G. Comellas · C. M. Rienstra
Center for Biophysics and Computational Biology, University of Illinois at Urbana-Champaign, 600 South Mathews Avenue, Urbana, IL 61801, USA

C. M. Rienstra
Department of Biochemistry, University of Illinois at Urbana-Champaign, 600 South Mathews Avenue, Urbana, IL 61801, USA

L. J. Mueller
Department of Chemistry, University of California, Riverside, CA 92521, USA

Initial applications of deuteration to solid-state NMR (SSNMR) have been reported in the literature, including both the study of protein dynamics and ^{1}H–^{1}H distance measurements, based on the detection of the deuterium and proton nucleus, respectively (Hologne et al. 2006; Linser et al. 2008). The relaxation and lines shape of the deuterium quadrupole, which are sensitive to the local dynamics, have also been used to obtain information on different motional behaviors (Hologne et al. 2006). The large gyromagnetic ratio of the ^{1}H nucleus provides high sensitivity to measure ^{1}H–^{1}H distances that are very useful for structure calculations, where deuteration has been used to eliminate the strong ^{1}H homonuclear dipolar couplings (Paulson et al. 2003). Recently, NMR samples with paramagnetic ion doping under fast MAS have shown enhanced sensitivity with fast data acquisition (Wickramasinghe et al. 2009). A set of low power ^{1}H decouplings also showed high resolution spectra of several proteins under fast MAS (Kotecha et al. 2007; Vijayan et al. 2009). Proton dilution from deuteration and back-exchange, combined with fast MAS and low power ^{1}H decoupling, made it possible to obtain enough ^{1}H–^{1}H distance constraints to calculate a full protein structure (Zhou and Rienstra 2008).

The application of deuterated samples for ^{13}C detection in typical solid-state NMR experiments, such as ^{13}C–^{13}C or ^{15}N–^{13}C correlations, has been investigated in the case of membrane proteins such as bacteriorhodopsin (Varga et al. 2007). Although some difficulties might be expected for ^{1}H–^{13}C cross-polarization (CP) with deuterated samples due to the dilution of the ^{1}H bath, Morcombe et al. demonstrated that CP efficiency is still reasonably efficient, the effect on the ^{1}H and ^{13}C T_1 relaxation times is surprisingly little, and no statistically significant broadening of the ^{13}C line widths was observed in the case of ubiquitin (Morcombe et al. 2005).

Here we present the effect of deuteration on chemical shifts, T_2 relaxations times, spin diffusion rates, and ^{1}H decoupling requirements for a deuterated protein, the beta-1 immunoglobulin binding domain of protein G (GB1), in high resolution ^{13}C-detected solid-state NMR spectra. Our results show significant improvement in T_2 relaxation times even with low proton-decoupling power that will make it possible to perform *J*-based SSNMR experiments (Chen et al. 2006, 2007) to improve resolution of non-crystalline samples. The improvement in the T_2 relaxation times and resolution will facilitate the sequential backbone assignments of large systems in which peak separation represents a big challenge, and exchangeable protons or water protons will enhance the selective detection of polar residues or residues that are close to water molecules. Therefore, the application of deuteration to SSNMR shows great potential in the structure determination of large protein systems that are of high interest and also in the evaluation of water accessibility on protein complexes and aggregates.

Experimental

^{1}H, ^{13}C, ^{15}N-labeled GB1 (U-CN-GB1) and ^{2}H, ^{13}C, ^{15}N-labeled GB1 (U-CDN-GB1) were prepared according to previously published procedures (Franks et al. 2005); (Zhou et al. 2007). The deuterated protein was purified in H_2O, so the exchangeable deuterons were replaced by protons. Nanocrystalline samples were precipitated with 2-methyl-pentane-2,4-diol (MPD) and isopropanol (IPA; Franks et al. 2005). A total of 18 mg material with 6 mg (1.0 μmol) U-CDN-GB1 was packed into a standard wall 3.2 mm MAS rotor with rubber disks for maintaining hydration. About 5 mg (0.9 μmol) U-CDN-GB1 and 4 mg solvents were packed into a 1.6 mm MAS rotor, and around 5 mg (0.9 μmol) U-CN-GB1 and 4 mg solvents were packed into another 1.6 mm MAS rotor.

NMR experiments were carried out on a 750 MHz Varian INOVA spectrometer with a 3.2 mm BioMAS probe (Stringer et al. 2005) and a 1.6 mm BioFastMAS probe (Varian, Inc.). For the BioMAS probe, the $\pi/2$ pulse widths for ^{1}H, ^{13}C, ^{15}N were 2.7, 4.5, 7.0 μs, respectively. For the BioFastMAS probe, the $\pi/2$ pulse widths for ^{1}H, ^{13}C were 1.7, 2.8 μs, respectively. The MAS rates were 12.5 kHz on the BioMAS probe and 18–40 kHz on the BioFastMAS probe. For 2D ^{13}C–^{13}C and ^{15}N–^{13}C experiments, the dipolar assisted rotational resonance (DARR) scheme (Takegoshi et al. 2001) was used for ^{13}C–^{13}C mixing. For 2D NcaCX experiments, a selective SPECIFIC CP (Baldus et al. 1998) was used for polarization transfer from ^{15}N to ^{13}C. Typical ^{1}H decoupling at 70 kHz was used for both t_1 and t_2 evolutions in 2D experiments at 12.5 kHz MAS. For 2D *J*-MAS CACO IPAP experiments (based on the CTUC COSY experiment Chen et al. 2006, 2007) acquired at 32 kHz MAS, 110 kHz SPINAL 64 (Fung et al. 2000) decoupling was used during the constant-time intervals and acquisition. Average echo T_2s

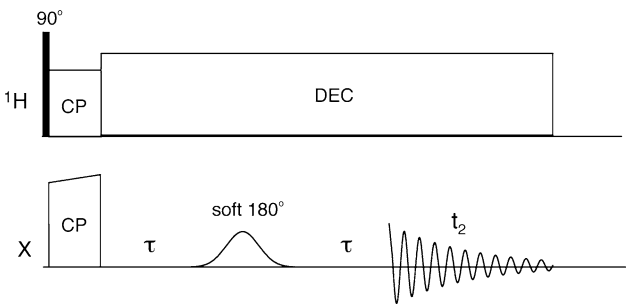

Fig. 1 Pulse sequence for the $^{13}C'$ and $^{13}C\alpha$ T_2 measurements of U-CDN-GB1 and U-CN-GB1

(typically referred to as T_2' (Lesage et al. 1999)) values for C′ and Cα at different decoupling conditions were measured using a 1D CP Hahn-echo (Hahn 1950) experiment with a 180° soft pulse on C′ or Cα resonance to remove the effect of ^{13}C–^{13}C *J*-couplings (Li et al. 2006; the pulse sequence is shown in Fig. 1). It has been reported that the linewidths of deuterated methyl groups can be improved by ^{2}H decoupling (Agarwal et al. 2006), so we measured T_2 values of C′, Cα and methyl groups of U-CDN-GB1 with low power ^{2}H WALTZ-16 (Shaka et al. 1983) decoupling (∼1.2 kHz) with a 1.6 mm ^{1}H–^{13}C–^{15}N–^{2}H magic-angle spinning probe on 500 MHz (^{1}H frequency) at 32 kHz MAS and found significant T_2 improvement in methyl groups as expected. Chemical shifts were referenced externally with adamantane with the downfield ^{13}C resonance of 40.48 ppm on the DSS scale (Morcombe and Zilm 2003).

2D spectra were processed with NMRPipe (Delaglio et al. 1995) and were analyzed with Sparky program (T. D. Goddard and D. G. Kneller, University of San Francisco). Back linear prediction and polynomial baseline correction were applied to the direct dimension. Zero

Table 1 Summary of T_2 values of $^{13}C'$ and $^{13}C\alpha$ of U-CDN-GB1 and U-CN-GB1

Sample	MAS rates (kHz)	^{1}H Dec scheme	^{1}H Dec power (kHz)	$^{13}C'$ (ms)	$^{13}C\alpha$ (ms)
U-CDN-GB1	12.5	None	0	8	9
		TPPM	70	18	13
		SPINAL	25	5	4
			50	25	24
			70	27	26
	18.0	XiX	7	10	11
			62	19	17
			120	34	25
		TPPM	7	10	11
			62	8	9
			120	20	18
		SPINAL	7	12	11
			62	11	12
			120	28	22
	26.0	XiX	7	12	12
			50	16	14
			120	35	23
		TPPM	7	12	14
			50	9	8
			120	35	21
		SPINAL	7	12	13
			50	8	8
			120	40	23
	36.0	XiX	7	25	19
			65	31	21
			120	50	26
		TPPM	7	25	19
			65	14	14
			120	30	21
		SPINAL	7	26	19
			65	23	20
			120	50	25
U-CN-GB1	12.5	TPPM	70	–	13
	18.0	XiX	43	22	12
		SPINAL	130	35	13
	40.0	XiX	43	22	12
		SPINAL	130	14	10

Generally, T_2' values were measured at three power levels (low, medium and high) with each decoupling scheme (XiX Detken et al. 2002, TPPM Bennett et al. 1995 and SPINAL Fung et al. 2000) under each MAS rate

filling and Lorentzian-to-Gaussian apodization were used for each dimensions before Fourier transformation. Detailed acquisition and processing parameters are included in figure captions.

Results and discussion

To evaluate the effect of deuteration on ^{13}C relaxation properties, ^{13}C CP Hahn-echo experiments were carried out for deuterated and protonated GB1 under different spinning rates and different ^{1}H decoupling sequences with various radio-frequency (RF) field strengths. The field strengths were selected to avoid rotary resonance conditions at high MAS rates by picking the local maximums of signal intensities while arraying the CW decoupling strengths (Ernst et al. 2003). Table 1 summarizes the ^{13}C T_2' values of U-CDN-GB1 and U-CN-GB1. At the moderate spinning rates (12.5 and 18 kHz), the ^{13}Cα T_2' of U-CDN-GB1 is almost twice the U-CN-GB1 with optimized SPINAL decoupling (26 vs. 13 ms). Even at the high spinning rate of 40 kHz, both the ^{13}Cα and ^{13}C$'$ T_2' of U-CDN-GB1 are much longer than for U-CN-GB1. Therefore, the removal of ^{13}C–^{1}H dipolar couplings by deuteration indeed improves the ^{13}C T_2' significantly. In terms of J-coupling effect from ^{2}H, we compared T_2 values of C$'$, Cα and methyl groups of U-CDN-GB1 under low power ^{2}H WALTZ-16 decoupling ($\sim$1.2 kHz) at 32 kHz MAS, and found no improvement in C$'$ (50 ms) and Cα (25 ms), but great enhancement in methyl groups from 21 to 50 ms. In addition to the echo T_2 values, the directly observed ^{13}C linewidths are greatly narrowed. Figure 2 and 3 show well-resolved ^{13}C–^{13}C 2D and NcaCX 2D spectra of U-CDN-GB1. Typical ^{13}C linewidths in the 2D spectra are 0.2–0.4 ppm, to which ^{13}C–^{13}C J-couplings, present in uniformly labeled samples, contribute 35–55 Hz (0.2–0.3 ppm). Especially apparent in the carbonyl region of the NcaCX 2D spectra (Fig. 3b) where ^{13}C$'$ linewidths are less than 0.2 ppm, so that some N–C$'$ crosspeaks actually show the splitting of $\sim$50 Hz corresponding to J_{COCA} (such as Y3, K4, D26, V39, F52, T55).

The assignments of U-CDN-GB1 were completed by comparing the 2D spectra with the ones of U-CN-GB1, using the published chemical shift of U-CN-GB1 and assuming that the upfield shift of ^{13}C chemical shift caused by deuterium is around 0.5–1.0 ppm. The ^{13}C$'$, ^{13}Cα, ^{13}Cβ, ^{15}N of all the residues have been assigned. As shown in the ^{13}C–^{13}C 2D spectrum with short 50 ms mixing time

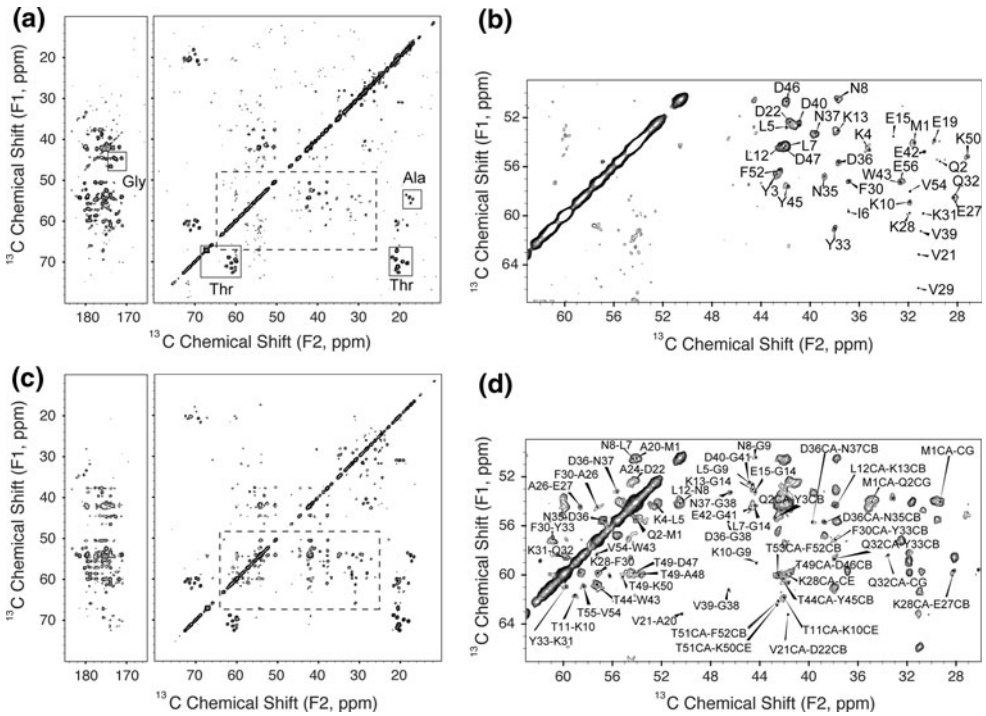

Fig. 2 ^{13}C–^{13}C 2D correlation spectra of U-CDN-GB1 at 12.5 kHz MAS with DARR mixing (BioMAS probe, 1.2 s pulse delay, 8 scans per row, maximum $t_1 = 15.36$ ms, maximum $t_2 = 20.48$ ms, ^{1}H carrier frequency set to 4.5 ppm, total 4.3–5.1 h). **a** 2D spectrum with 50 ms DARR mixing. *Dashed rectangle* indicates the expanded region. *Solid rectangles* indicate well-resolved peaks from Gly, Ala and Thr. **b** Expanded spectrum of intraresidual Cα-Cβ correlations with 50 ms DARR mixing (labels include only the residue numbers). **c** 2D spectrum with 300 ms DARR mixing. *Dashed rectangle* indicates the expanded region. **d** Expanded spectrum of interresidual Cα-Cα and Cα-Cβ correlations with 300 ms DARR mixing (Cα-Cα correlations labels only include the residue numbers). Both data were processed with 20 and 20 Hz net line broadening in each dimension

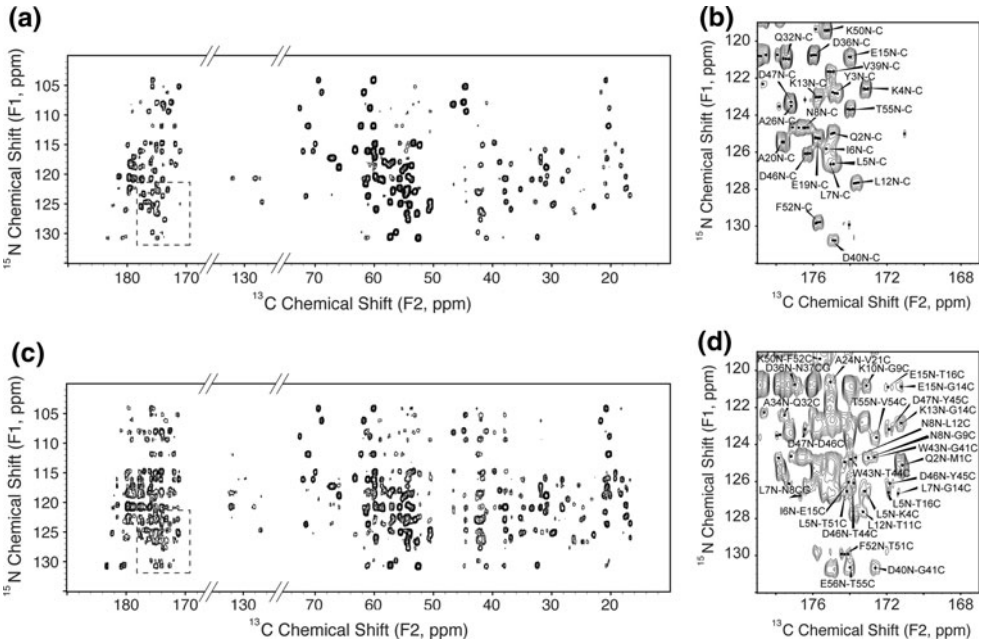

Fig. 3 NcaCX 2D spectra of U-CDN-GB1 at 12.5 kHz with ^{13}C–^{13}C DARR mixing (BioMAS probe, 1.2 s pulse delay, 64 scans per row, 4.8 ms NC SPECIFIC CP, maximum $t_1 = 16$ ms, maximum $t_2 = 20.48$ ms, ^{1}H carrier frequency set to 8.3 ppm, total 3–3.5 h). **a** NcaCX 2D spectrum with 50 ms DARR mixing. **b** Expanded region in the dashed rectangle in **a** shows intraresidual N–C′ correlations. **c** NcaCX 2D spectrum with 300 ms DARR mixing. **d** Expanded region in the dashed rectangle in **c** shows interresidual N–C′ correlations. Both data were processed with 20 and 10 Hz net line broadening in ^{15}N and ^{13}C dimension, respectively

Table 2 Summary of chemical shift differences ($\Delta\delta(D) = \delta(D) - \delta(H)$) between U-CN-GB1 and UCDN-GB1

Residues	Site	Environment	$\Delta\delta$(D) (ppm)	$\{d_{1b}, d_{2b}, d_{3b}\}$	$\Delta\delta(D)_{calc}$ (ppm)
		No deuteron			
All	C′	CO(CD,NH)	−0.103 ± 0.180		
Asp, Asn	Cγ	CO(CD_2,NH_2)	−0.026 ± 0.177		
Glu, Gln	Cδ	CO(CD_2, NH_2)	0.012 ± 0.115		
All	N	NH(CD)	−0.299 ± 0.128		−0.3[a]
		C with one deuteron			
Thr	Cα	CD(CDOH,NH)	−0.276 ± 0.048	{1,1,3}	−0.63
Ala	Cα	CD(CD_3,NH)	−0.336 ± 0.082	{1,3,0}	−0.68
Val, Ile	Cα	CD(CD,NH)	−0.344 ± 0.065	{1,1,6}	−0.84
Asp, Asn, Phe, Tyr, Trp	Cα	CD(CD_2,NH)	−0.282 ± 0.117	{1,2,0}	−0.55
Leu	Cα	CD(CD_2,NH)	−0.285 ± 0.056	{1,2,1}	−0.69
Glu, Gln, Lys, Met	Cα	CD(CD_2,NH)	−0.366 ± 0.045	{1,2,2}	−0.76
Thr	Cβ	CD(CD,CD_3,OH)	−0.620 ± 0.482	{1,4,0}	−0.81
Val	Cβ	CD(CD_3,CD_3)	−0.951 ± 0.049	{1,7,0}	−1.20
		C with two deuterons			
Gly	Cα	CD_2(NH)	−0.277 ± 0.117	{2,0,0}	−0.39[a]
Asp, Asn, Phe, Tyr, Trp	Cβ	CD_2(CD,C)	−0.620 ± 0.482	{2,1,0}	−0.71
Glu, Gln, Met	Cβ	CD_2(CD,CD_2)	−0.892 ± 0.074	{2,3,0}	−0.97
Leu	Cβ	CD_2(CD,CD_2)	−0.946 ± 0.051	{2,2,6}	−1.26
Lys	Cβ	CD_2(CD,CD_2)	−0.971 ± 0.064	{2,3,2}	−1.11
Glu, Gln	Cγ	CD_2(CD_2,C)	−0.694 ± 0.113	{2,2,1}	−0.91
Lys	Cγ	CD_2(CD_2,CD_2)	−1.137 ± 0.067	{2,4,3}	−1.31
Lys	Cδ	CD_2(CD_2,CD_2)	−1.258 ± 0.480	{2,4,2}	−1.1
Lys	Cε	CD_2(CD_2,NH_3)	−0.621 ± 0.346	{2,2,2}	−0.98
		C with three deuterons			
Ala	Cβ	CD_3(CD)	−0.776 ± 0.063	{3,1,0}	−1.00
Thr	Cγ	CD_3(CD–CD)	−0.886 ± 0.075	{3,1,1}	−1.07
Val	Cγ	CD_3(CD–CD_3)	−0.937 ± 0.093	{3,1,4}	−1.28
Leu	Cδ	CD_3(CD)	−1.181 ± 0.130	{3,1,5}	−1.35

$\Delta\delta(D)_{calc}$ are calculated with Eq. (1), where $^1\Delta\delta(D) = -0.29$, $^2\Delta\delta(D) = -0.13$ and $^3\Delta\delta(D) = -0.07$ ppm (Venters et al. 1996)

[a] ^{15}N and $^{13}C\alpha_{Gly}$ chemical shifts were separately measured

(Fig. 2a), there are clearly resolved Ala Cα-Cβ, Gly Cα-C′, Thr Cα-Cβ and Cβ-Cγ2 crosspeaks. An expansion of the Cα-Cβ crosspeaks of all other residues is shown in Fig. 2b. The residues that are in β-strand have stronger Cα-Cβ peaks than those in helix, and the peaks from polar and aromatic residues have higher intensities than those from nonpolar residues. At long 300 ms mixing time (Fig. 2c, d), the spectrum showed more correlations between the sidechains and backbone carbons of polar residues, and also some inter-residual correlations in which at least one residue is polar or aromatic. Similar crosspeak patterns occurred in NcaCX 2D spectra (Fig. 3). Almost all the N–C′, N–Cα, N–Cβ peaks are well resolved in the spectrum at short mixing time, with some N–Cγ (Asn, Asp), N–Cδ (Gln, Glu) and N–Cε (Lys) peaks for the residues with exchangeable-proton sidechains. At the long mixing time, inter-residue N–C peaks show up and mainly involved with polar residues. In the expanded region of NcaCX 2D spectrum with 300 ms mixing (Fig. 3d), crosspeaks between Leu and other residues are clearly weaker than those between polar residues. Furthermore, some crosspeaks appear in the region of 110–140 ppm of ^{13}C chemical shift, corresponding to the correlations between amide nitrogens and sidechain carbons of Y3, Y33, Y45 and W43, which also have exchangeable protons on the side chains. Overall, most sidechain ^{13}C of polar residues and some of the nonpolar and aromatic residues were assigned, and the deviations of these assignments were within 0.1 ppm. Therefore, the deuterated protein samples not only maintain the capability of assigning all the backbone resonances that are important for determining the secondary structures, but also strengthen the selection of sidechains of polar residues that are closely related to protein functions or interactions between proteins. Particularly in solid-state NMR, this feature would be valuable for assigning loop regions or channel lining interfaces of membrane proteins, since those regions are usually abundant of polar residues.

To confirm our assumptions and characterize in more detail the upfield isotope shifts from deuterium, we compared the chemical shifts of U-CDN-GB1 and U-CN-GB1, as summarized in Table 2. $\Delta\delta(\mathrm{D})_{\mathrm{calc}}$ are calculated by the equation (Venters et al. 1996):

$$\Delta\delta(\mathrm{D})_{\mathrm{calc}} = {}^{1}\Delta\delta(\mathrm{D})d_{1\mathrm{b}} + {}^{2}\Delta\delta(\mathrm{D})d_{2\mathrm{b}} + {}^{3}\Delta\delta(\mathrm{D})d_{3\mathrm{b}} \qquad (1)$$

where ${}^{\mathrm{n}}\Delta\delta(\mathrm{D})$ represents the n-bond isotope effect per deuteron and d_{nb} is the number of deuterons n bonds away from the detected nucleus. The average deuterium effects are ~0.1 ppm for ^{13}C′, ~0.3 ppm for ^{13}Cα and ~0.9 ppm for ^{13}Cβ. Generally, the deuterium effects in solid-state NMR are slightly smaller (0.1–0.2 ppm) than the values in solution NMR. For each site, the deuterium effects are mostly consistent (deviations within 0.1 ppm), except a few outliers with deviations larger than 0.4 ppm (Thr, Trp, Tyr ^{13}Cβ, Lys ^{13}Cδ and ^{13}Cε). Such deviations were also observed in solution NMR (Venters et al. 1996), which could result from subtle environmental changes around these sites that are next to either hydroxyl groups, amine groups or aromatic rings.

While all multidimensional experiments gain from the increase in signal power associated with longer T_2 values, scalar-coupling-driven correlation experiments will additionally benefit from the slower decoherence rates during the relatively long echo periods necessary for coherence transfer through the J coupling. Indeed, during the last decade a growing number of 2D and 3D correlation experiments have emerged that make use of the indirect spin–spin coupling to map out through-bond connectivity in solid-state proteins (Chen et al. 2007; Chen et al. 2006; De Paepe et al. 2003; Detken et al. 2001; Linser et al. 2008). The vast majority of these experiments have been implemented under conditions of high-power proton decoupling (>150 kHz), where the value of the echo T_2' is maximized (De Paepe et al. 2003). Deuteration will allow the use of lower power decouplings while maintaining longer T_2' values (Agarwal et al. 2006), as we exploit in the implementation of the J-MAS CACO IPAP correlation experiment (Chen et al. 2006, 2007) shown in Fig. 4. This J-based correlation spectrum was acquired at 32 kHz MAS with only moderate (110 kHz, 75% of the full power—150 kHz) proton decoupling. The combination of the

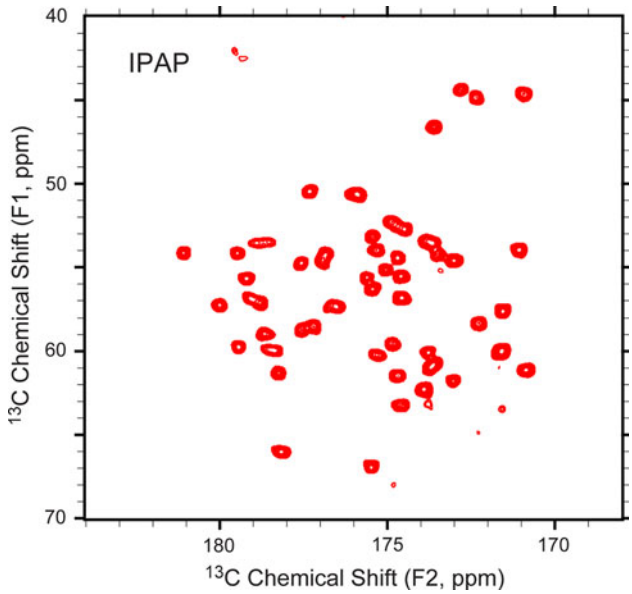

Fig. 4 J-MAS CACO IPAP spectrum of UCDN-GB1 at 32 kHz (BioFastMAS probe, 1.5 s pulse delay, 16 scans per row, constant time interval $\tau_1 = \tau_2 = 4.5$ ms, maximum $t_1 = 8.5$ ms, maximum $t_2 = 20.48$ ms, ^{1}H carrier frequency set to 4.5 ppm, total 7.5 h). It was the added spectrum of IP and AP spectra. The data were processed with 5 Hz net line broadening in both dimensions

constant-time evolution in the indirect dimension (Chen et al. 2006, 2007) and the in-phase anti-phase selection in the direct dimension (Bermel et al. 2005) leads to a highly resolved 2D spectrum and deuteration paired with low power proton decoupling that is clearly compatible even with challenging *J*-based transfer experiments.

One significant practical aspect of these studies is that the ^{1}H–^{13}C CP conditions for the U-CDN-GB1 sample are much more sensitive than those for U-CN-GB1. This is the case even with a large tangent amplitude ramp applied, and thus the CP amplitudes need careful optimization under the condition where 2D experiments would be performed. Moreover, the overall instrumental stability is critical, in addition to the optimization of ^{1}H decoupling to achieve optimal T_2' values. Figure 5 shows that U-CDN-GB1 Cα signal intensities had less variation with different pulse widths and phase angles of SPINAL 64 decoupling that those of TPPM decoupling. Therefore, SPINAL decoupling is much less sensitive to pulse width and phase angle than TPPM decoupling. We also found that SPINAL decoupling is less sensitive to ^{1}H carrier frequency than TPPM decoupling (data not shown). Figure 6 compares the NcaCX 2D spectra of U-CDN-GB1 at 12.5 kHz MAS with SPINAL and TPPM decouplings. The ^{15}N linewidths are significantly better using SPINAL decoupling than using TPPM decoupling (0.5 vs. 1.2 ppm for D40 ^{15}N). Therefore, SPINAL decoupling is a better choice for deuterated protein samples. In addition, low-power XiX decoupling provides reasonable T_2' values at fast MAS (Table 1), and thus it is also a viable choice in fast spinning regime.

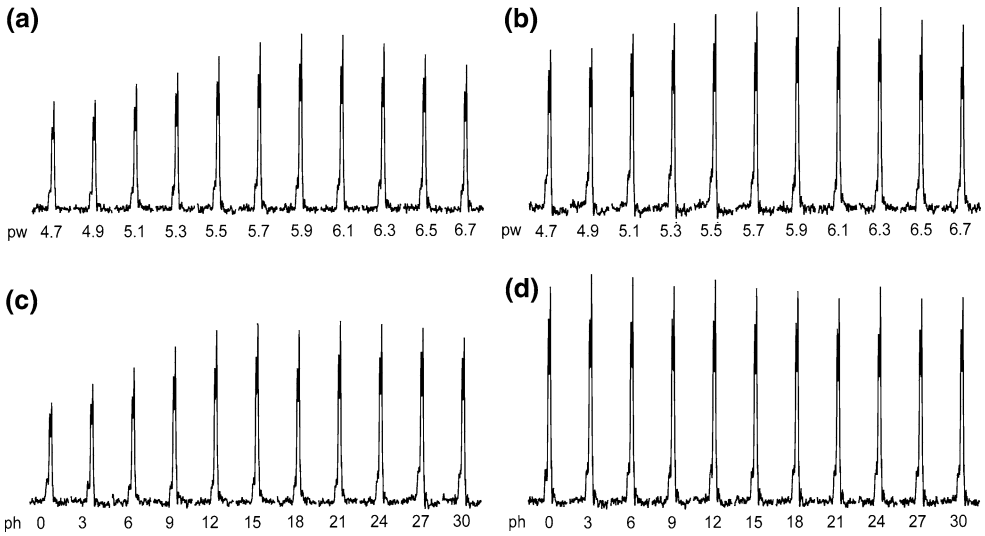

Fig. 5 ^{13}C CP Hahn-echo spectra (Cα region shown) of U-CDN-GB1 at 18 kHz MAS with TPPM and SPINAL decoupling schemes: **a** TPPM decoupling as a function of the pulse width (pw in μs); **b** SPINAL-64 decoupling as a function of the pulse width (pw in μs); **c** TPPM decoupling as a function of the phase; **d** SPINAL-64 decoupling as a function of the phase (ph); The ^{1}H carrier frequency was set to 8.3 ppm. The decoupling strength was 95 kHz for both schemes. The Hahn-echo time was 8.89 ms

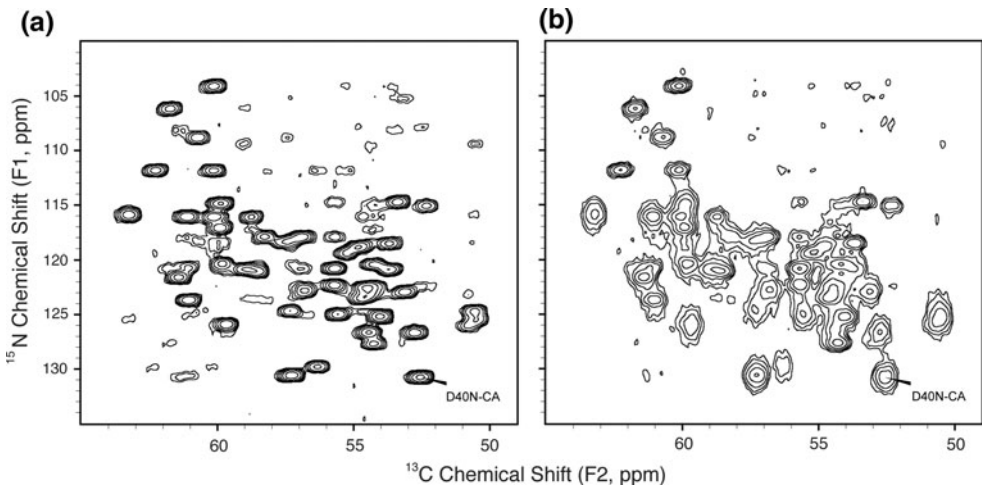

Fig. 6 NcaCX 2D spectra of U-CDN-GB1 with 100 ms DARR mixing under SPINAL and TPPM ^{1}H decouplings (BioMAS probe, 1.2 s pulse delay, 64 scans per row, 4.8 ms NC SPECIFIC CP, maximum $t_1 = 16$ ms, maximum $t_2 = 20.48$ ms, total 3–3.5 h). **a** N–Cα region of NcaCX 2D spectrum using 70 kHz SPINAL decoupling in both t_1 and t_2 evolutions ($\tau_p = 7.2$ μs, $\phi = 6°$, $\alpha = 10°, \beta = 20°$). ^{1}H carrier frequency was set to amide ^{1}H frequency (8.3 ppm). **b** N–Cα region of NcaCX 2D spectrum using 70 kHz TPPM decoupling in both t_1 and t_2 evolutions ($\tau_p = 6.6$ μs, $\phi = 12°$). ^{1}H carrier frequency was set to amide ^{1}H frequency (8.3 ppm)

Conclusions

We have demonstrated ^{13}C-detected solid-state NMR spectroscopy of deuterated GB1. Deuteration provides a significant improvement in $^{13}C\alpha$ T_2' by eliminating the ^{13}C–^{1}H dipolar couplings. T_2' enhancement makes experiments that require long T_2' values feasible, such as *J*-based experiments, especially for large proteins in higher magnetic field. Unique crosspeak patterns that result from exchangeable protons on sidechains of polar residues reduce the overlap in the methylene and methyl regions and provides easier identification of polar residues in large proteins, which usually play important roles in protein functions and/or in the interactions with other proteins.

Acknowledgments The authors thank the National Institute of Health (NIGMS GM075937 and GM073770, S10RR023677) and the National Science Foundation (CHE-0848607) for funding, the Caja Madrid Foundation and Agusti Pedro Pons graduate fellowships to GC, and John J. Shea and John M. Boettcher for the sample preparation.

References

Agarwal V, Diehl A, Skrynnikov N, Reif B (2006) High resolution ^{1}H detected ^{1}H, ^{13}C correlation spectra in MAS solid-state NMR using deuterated proteins with selective ^{1}H, ^{2}H isotopic labeling of methyl groups. J Am Chem Soc 128(39):12620–12621

Baldus M, Petkova AT, Herzfeld J, Griffin RG (1998) Cross polarization in the tilted frame: assignment and spectral simplification in heteronuclear spin systems. Mol Phys 95(6):1197–1207

Bennett AE, Rienstra CM, Auger M, Lakshmi KV, Griffin RG (1995) Heteronuclear decoupling in rotating solids. J Chem Phys 103(16):6951–6958

Bermel W, Bertini I, Duma L, Felli IC, Emsley L, Pierattelli R, Vasos PR (2005) Complete assignment of heteronuclear protein resonances by protonless NMR spectroscopy. Angew Chem Int Ed 44(20):3089–3092

Chen LL, Olsen RA, Elliott DW, Boettcher JM, Zhou DH, Rienstra CM, Mueller LJ (2006) Constant-time through-bond ^{13}C correlation spectroscopy for assigning protein resonances with solid-state NMR spectroscopy. J Am Chem Soc 128(31):9992–9993

Chen LL, Kaiser JM, Lai JF, Polenova T, Yang J, Rienstra CM, Mueller LJ (2007) J-based 2D homonuclear and heteronuclear correlation in solid-state proteins. Magn Reson Chem 45:S84–S92

De Paepe G, Giraud N, Lesage A, Hodgkinson P, Bockmann A, Emsley L (2003) Transverse dephasing optimized solid-state NMR spectroscopy. J Am Chem Soc 125(46):13938–13939

Delaglio F, Grzesiek S, Vuister GW, Zhu G, Pfeifer J, Bax A (1995) Nmrpipe: a multidimensional spectral processing system based on unix pipes. J Biomol NMR 6(3):277–293

Detken A, Hardy EH, Ernst M, Kainosho M, Kawakami T, Aimoto S, Meier BH (2001) Methods for sequential resonance assignment in solid, uniformly ^{13}C, ^{15}N labelled peptides: quantification and application to antamanide. J Biomol NMR 20(3):203–221

Detken A, Hardy EH, Ernst M, Meier BH (2002) Simple and efficient decoupling in magic-angle spinning solid-state NMR: the XiX scheme. Chem Phys Lett 356(3–4):298–304

Ernst M, Samoson A, Meier BH (2003) Low-power XiX decoupling in MAS NMR experiments. J Magn Reson 163(2):332–339

Franks WT, Zhou DH, Wylie BJ, Money BG, Graesser DT, Frericks HL, Sahota G, Rienstra CM (2005) Magic-angle spinning solid-state NMR spectroscopy of the beta-1 immunoglobulin binding domain of protein G (GB1): ^{15}N and ^{13}C chemical shift assignments and conformational analysis. J Am Chem Soc 127(35):12291–12305

Fung BM, Khitrin AK, Ermolaev K (2000) An improved broadband decoupling sequence for liquid crystals and solids. J Magn Reson 142(1):97–101

Gardner KH, Kay LE (1998) The use of ^{2}H, ^{13}C, ^{15}N multidimensional NMR to study the structure and dynamics of proteins. Annu Rev Biophys Biomol Struct 27:357–406

Hahn EL (1950) Spin echoes. Phys Rev 80(4):580–594

Hologne M, Chevelkov V, Reif B (2006) Deuterated peptides and proteins in MAS solid-state NMR. Prog Nucl Mag Res Sp 48:211–232

Kotecha M, Wickramasinghe NP, Ishii Y (2007) Efficient low-power heteronuclear decoupling in ^{13}C high-resolution solid-state NMR under fast magic angle spinning. Magn Reson Chem 45(S1):S221–S230

Lesage A, Bardet M, Emsley L (1999) Through-bond carbon-carbon connectivities in disordered solids by NMR. J Am Chem Soc 121(47):10987–10993

Li Y, Wylie BJ, Rienstra CM (2006) Selective refocusing pulses in magic-angle spinning NMR: characterization and applications to multi-dimensional protein spectroscopy. J Magn Reson 179(2):206–216

Linser R, Fink U, Reif B (2008) Proton-detected scalar coupling based assignment strategies in MAS solid-state NMR spectroscopy applied to perdeuterated proteins. J Magn Reson 193(1):89–93

Morcombe CR, Zilm KW (2003) Chemical shift referencing in MAS solid state NMR. J Magn Reson 162(2):479–486

Morcombe CR, Gaponenko V, Byrd RA, Zilm KW (2005) 13C CPMAS spectroscopy of deuterated proteins: CP dynamics, line shapes, and T_1 relaxation. J Am Chem Soc 127(1):397–404

Paulson EK, Morcombe CR, Gaponenko V, Dancheck B, Byrd RA, Zilm KW (2003) High-sensitivity observation of dipolar exchange and NOEs between exchangeable protons in proteins by 3D solid-state NMR spectroscopy. J Am Chem Soc 125(47):14222–14223

Shaka AJ, Keeler J, Frenkiel T, Freeman R (1983) An improved sequence for broad-band decoupling—waltz-16. J Magn Reson 52(2):335–338

Stringer JA, Bronnimann CE, Mullen CG, Zhou DHH, Stellfox SA, Li Y, Williams EH, Rienstra CM (2005) Reduction of RF-induced sample heating with a scroll coil resonator structure for solid-state NMR probes. J Magn Reson 173(1):40–48

Takegoshi K, Nakamura S, Terao T (2001) 13C–1H dipolar-assisted rotational resonance in magic-angle spinning NMR. Chem Phys Lett 344(5–6):631–637

Varga K, Aslimovska L, Parrot I, Dauvergne M-T, Haertlein M, Forsyth VT, Watts A (2007) NMR crystallography: the effect of deuteration on high resolution ^{13}C solid state NMR spectra of a 7-TM protein. Biochim Biophys Acta 1768:3029–3035

Venters RA, Farmer BT 2nd, Fierke CA, Spicer LD (1996) Characterizing the use of perdeuteration in NMR studies of large proteins: ^{13}C, ^{15}N and ^{1}H assignments of human carbonic anhydrase II. J Mol Biol 264(5):1101–1116

Vijayan V, Demers JP, Biernat J, Mandelkow E, Becker S, Lange A (2009) Low-power solid-state NMR experiments for resonance assignment under fast magic-angle spinning. ChemPhysChem (published online Jul 14)

Wickramasinghe NP, Parthasarathy S, Jones CR, Bhardwaj C, Long F, Kotecha M, Mehboob S, Fung LWM, Past J, Samoson A, Ishii Y (2009) Nanomole-scale protein solid-state NMR by breaking intrinsic ^{1}H T_1 boundaries. Nat Methods 6(3): 215–218

Zhou DH, Rienstra CM (2008) Rapid analysis of organic compounds by proton-detected heteronuclear correlation NMR spectroscopy at 40 kHz magic-angle spinning. Angew Chem Int Ed 47:7328–7331

Zhou DH, Shea JJ, Nieuwkoop AJ, Franks WT, Wylie BJ, Mullen C, Sandoz D, Rienstra CM (2007) Solid-state protein-structure determination with proton-detected triple-resonance 3D magic-angle spinning NMR spectroscopy. Angew Chem Int Ed 46(44):8380–8383